Construction and Building Materials 364 (2023) 129923

Contents lists available at ScienceDirect

Construction and Building Materials

journal homepage: www.elsevier.com/locate/conbuildmat

Comparative study on the bond performance of near-surface mounted fiber-reinforced polymer bars

Omar Aljidda [a], Ahmed El Refai [a,*], Wael Alnahhal [b]

[a] Department of Civil and Water Engineering, Laval University, Quebec City, Quebec, G1V 0A6, Canada
[b] Department of Civil and Architectural Engineering, Qatar University, P.O. Box 2713, Doha, Qatar

ARTICLE INFO

Keywords:
Near-surface mounted technique
Fiber-reinforced polymer
Pullout
Bond
Slip
Basalt
Strengthening
Adhesive
Epoxy
BPE model

ABSTRACT

This paper presents the experimental and analytical results of a large study on the bond performance of near-surface mounted (NSM) fiber-reinforced polymer (FRP) bars. The investigated parameters included the bar material (basalt-FRP (BFRP), glass-FRP (GFRP), carbon-FRP (CFRP), and stainless steel (SS) bars), the bar surface configuration (deformed and sand-coated bars), the filling adhesive (NSM-Gel, Sikadur-30, and Sika Grout-214), and the bonded length of the bar (6, 12, and 24 times its diameter). Sixty-six C-shape concrete specimens were tested under direct pullout loading configuration. The bond strength, the free-end and loaded-end slip, the strains in the NSM bar, and the modes of failure of the tested specimens are reported and discussed. The NSM-Gel adhesive outperformed other adhesives in developing the bond strength of the tested specimens regardless of their bar material. Both the deformed and sand-coated NSM-BFRP and GFRP bars showed almost similar bond strengths while the NSM-CFRP bars showed the highest strengths. The images obtained from the scanning electron microscope confirmed the obtained results in terms of the modes of failure and the bond failure mechanism. Analytically, the BPE model was calibrated using the experimental results to describe the bond stress-slip relationships of the FRP bars.

1. Introduction and background

Near-surface mounted (NSM) technique necessitates the embedment of reinforcing bars or strips in grooves formerly cut into the concrete cover and adhered to the surrounding concrete with an appropriate filling material (the adhesive). Fiber-reinforced polymer (FRP) bars are widely used as NSM bars due to their corrosion resistance and their exceptional tensile strength [1–3]. Previous studies demonstrated that NSM-FRP bars could provide excellent anchoring capacity resulting in high resistance to debonding, hence a high percentage of their tensile strength could be deployed [4–7]. The stress transfer and the interaction mechanisms between the bar, the adhesive, and the surrounding concrete occur via two interfaces, namely, (a) the cylindrical interface between the NSM bar and the adhesive and (b) the rectangular interface between the adhesive and the surrounding concrete. Good bond at both interfaces allows for the stress transfer between the FRP bars, the adhesive, and the concrete and ensures a sound composite behavior.

The performance of the NSM-FRP bars depends on many parameters including the groove size, the texture of the bar surface, the bar diameter, the bonded length of the bar, the adhesive, and most importantly, the bond mechanism at the bar-adhesive and the concrete-adhesive interfaces [6,8–17]. Sharaky et al. [16] reported that increasing the groove depth and width increased the failure load of the NSM-FRP bars regardless of the surface treatment of the bars or their materials. Increasing the bar diameter of NSM-CFRP bars from 8 to 9 mm increased their bond strength by 22 % whereas increasing the diameter of NSM-GFRP bars from 8 to 12 mm increased their strength by 72 %. Moreover, sand-coated and ribbed NSM bars usually offer high bond strength due to the roughened texture of the bar in contact with the epoxy adhesive [8,14]. Lee et al. [14] also reported that the use of spirally-wound and sand coated NSM-GFRP and CFRP bars showed better bond performance compared to smooth surface bars. Wang and Cheng [18] confirmed those results and reported that NSM-CFRP bars having sand-coated and spirally wound texture outperformed both the roughened and sand-coated bars in terms of bond strength. On the other hand, Soliman et al. [19] reported that NSM-CFRP and GFRP bars adhered to concrete using epoxy adhesives showed 40 to 56 % gain in their bond strength compared to their counterparts with cementitious adhesives. The authors also reported that the concrete splitting failure was the dominant failure mode in most of the specimens with epoxy adhesives

* Corresponding author.
E-mail addresses: omar.aljidda.1@ulaval.ca (O. Aljidda), ahmed.elrefai@gci.ulaval.ca (A. El Refai), wael.alnahhal@qu.edu.qa (W. Alnahhal).

https://doi.org/10.1016/j.conbuildmat.2022.129923
Received 6 August 2022; Received in revised form 19 November 2022; Accepted 27 November 2022
Available online 8 December 2022

Table 1
Test matrix of the pullout experimental program.

Specimen (No. of specimens)	NSM bar		Bonded length	Groove adhesive
	Material	Surface		
Deformed BFRP specimens				
B-D-6-NG (1)	BFRP	Deformed	$6d_b$	NSM-Gel
B-D-6-SD (1)			$6d_b$	Sikadur-30
B-D-12-NG (3)			$12d_b$	NSM-Gel
B-D-12-SD (3)			$12d_b$	Sikadur-30
B-D-12-SG (3)			$12d_b$	Sika grout-214
B-D-24-NG (1)			$24d_b$	NSM-Gel
B-D-24-SD (1)			$24d_b$	Sikadur-30
Sand-coated BFRP specimens				
B-SC-6-NG (1)	BFRP	Sand-coated	$6d_b$	NSM-Gel
B-SC-6-SD (1)			$6d_b$	Sikadur-30
B-SC-12-NG (3)			$12d_b$	NSM-Gel
B-SC-12-SD (3)			$12d_b$	Sikadur-30
B-SC-24-NG (1)			$24d_b$	NSM-Gel
B-SC-24-SD (1)			$24d_b$	Sikadur-30
Deformed GFRP specimens				
G-D-6-NG (1)	GFRP	Deformed	$6d_b$	NSM-Gel
G-D-6-SD (1)			$6d_b$	Sikadur-30
G-D-12-NG (3)			$12d_b$	NSM-Gel
G-D-12-SD (3)			$12d_b$	Sikadur-30
G-D-24-NG (1)			$24d_b$	NSM-Gel
G-D-24-SD (1)			$24d_b$	Sikadur-30
Sand-coated GFRP specimens				
G-SC-6-NG (1)	GFRP	Sand-coated	$6d_b$	NSM-Gel
G-SC-6-SD (1)			$6d_b$	Sikadur-30
G-SC-12-NG (3)			$12d_b$	NSM-Gel
G-SC-12-SD (3)			$12d_b$	Sikadur-30
G-SC-24-NG (1)			$24d_b$	NSM-Gel
G-SC-24-SD (1)			$24d_b$	Sikadur-30
Deformed CFRP specimens				
C-D-6-NG (1)	CFRP	Deformed	$6d_b$	NSM-Gel
C-D-6-SD (1)			$6d_b$	Sikadur-30
C-D-12-NG (3)			$12d_b$	NSM-Gel
C-D-12-SD (3)			$12d_b$	Sikadur-30
C-D-24-NG (1)			$24d_b$	NSM-Gel
C-D-24-SD (1)			$24d_b$	Sikadur-30
Deformed SS specimens				
SS-D-6-NG (1)	SS	Deformed	$6d_b$	NSM-Gel
SS-D-6-SD (1)			$6d_b$	Sikadur-30
SS-D-12-NG (3)			$12d_b$	NSM-Gel
SS-D-12-SD (3)			$12d_b$	Sikadur-30
SS-D-12-SG (3)			$12d_b$	Sika grout-214
SS-D-24-NG (1)			$24d_b$	NSM-Gel
SS-D-24-SD (1)			$24d_b$	Sikadur-30

whereas specimens with cementitious adhesives failed due to the adhesive splitting at the concrete-adhesive interface. In a more recent study, Cruz et al. [20] investigated the influence of using stiff and flexible epoxy adhesives with NSM-CFRP strips. The experimental results showed that specimens with stiff adhesives recorded the highest bond strength and failed due to debonding at the strip-adhesive interface or by the rupture of the strips whereas specimens with flexible adhesives failed by debonding of the strip along the adhesive interface.

It can be noticed that most of the previous studies have been devoted to assessing the bond performance of NSM-GFRP and CFRP bars/strips [4,6,8–13,21–24]. Despite the large number of studies reported, an obvious lack of studies on the use of basalt-FRP (BFRP) bars in NSM applications can be observed [25]. BFRP bars have emerged recently as promising alternatives to the conventional GFRP bars. Several studies have been conducted to study their bond performance [26–29] and bond durability [30–33] and confirmed their excellent short- and long-term bond performance. Other studies have reported on their efficiency as flexural reinforcement [34–39], shear reinforcement [40–43], and compression reinforcement [44,45] for RC structures.

This study is part of a comprehensive research program aiming at evaluating the feasibility of using the BFRP bars in NSM flexural applications versus the conventional CFRP and GFRP bars in addition to stainless steel (SS) bars. This paper reports on the first phase of the experimental program in which pullout tests were conducted while investigating various parameters. The findings of this study were deemed to be crucial prior recommending the use of BFRP bars in NSM applications.

2. Experimental program

The experimental program consisted of testing 66C-shaped concrete specimens under pull-out loading. The test matrix was designed to investigate the most influencing parameters that are known to affect the bond of the NSM-FRP bars. The investigated parameters included the material of the bar (BFRP, GFRP, CFRP, and SS bars), the bar surface (deformed and sand-coated surfaces), and the bonded length of the bar (6, 12, and 24 times the bar diameter, d_b). In addition, three types of groove filling material were used namely, the NSM-Gel and Sikadur-30, which are both epoxy-based adhesives, and the Sika grout-214, which is a cementitious grout.

Table 1 shows the test matrix of the experimental program. The specimens are identified with the following notation: X-Y-00-Z, where the first letter, X, refers to the bar type ('B' for BFRP, 'G' for GFRP, 'C' for CFRP, and 'SS' for stainless steel bars). The second letter, Y, denotes the surface configuration of the bar ('SC' for sand-coated and 'D' for deformed bars), while the last letter, Z, refers to the type of the filling material type ('NG' for NSM-Gel epoxy, 'SD' for Sikadur-30 epoxy, and 'SG' for Sika grout-214 cementitious grout). The two digits in each specimen's label define the bonded length of the bar, expressed as a multiple of its nominal diameter, d_b. All NSM bars used in this study

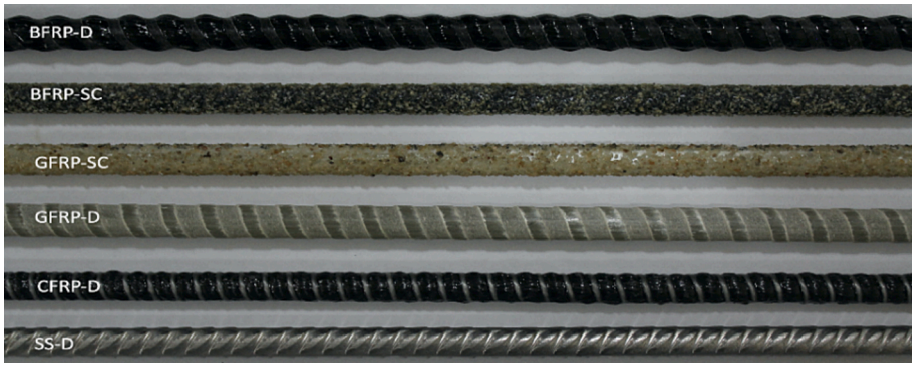

Fig. 1. Types of NSM bars used in this study (D = deformed, SC = sand-coated).

Table 2
Mechanical properties of the NSM bars used in this study.

Bar type	Nominal bar diameter [a]	Measured bar diameter [b]	Bar surface	Modulus of elasticity (GPa)	Tensile strength (MPa)	Ultimate strain %
Deformed bars						
SS	10	9.98	Deformed	200	587	0.29
BFRP	10	9.61	Deformed	52	1200	2.31
CFRP	10	9.91	Deformed	120	1800	1.5
GFRP	10	11.15	Deformed	60	1100	1.8
Sand-coated bars						
GFRP	10	10.28	Sand-coated	59.1	1146	1.94
BFRP	10	9.70	Sand-coated	57.5	1277	2.22

[a] As reported by the manufacturer.
[b] Average data from three immersion tests according to ISO10406-15 [50].

Table 3
Properties of the filling adhesives used in this study (as reported by the manufacturers).

Material	Type	Modulus of elasticity (MPa)	Shear strength (MPa)	Cure time
NSM-Gel	Epoxy	1682	27.2	14 days
Sikadur-30	Epoxy	9600	18	7 days
Sika grout-214	Cement grout	37,000	–	28 days

had a nominal diameter of 10 mm. Specimens with bonded length of 12 d_b had three replicates. The test results of those replicates were consistent and showed slight discrepancy in terms of the pullout strength and displacement except a few tests that showed peculiar results, which were eliminated from the analysis. Therefore, to minimize the number of the tested specimens, only one test was performed on specimens with bonded lengths of 6 d_b and 24 d_b.

2.1. Material properties

All specimens were cast using ready-mixed concrete with a target compressive strength of 50 MPa. This relatively high strength concrete was used to better employ the high tensile strength of the FRP bars and to prevent the splitting of concrete before developing the bond strength of the bars. An average compressive strength of 53.5 MPa was obtained by testing three standard concrete cylinders (200 × 100 mm) in accordance with ASTM C39-21 [48] whereas an average tensile strength of 5.8 MPa was determined by testing three concrete prisms (100 × 100 × 500 mm) according to ASTM C78-21 [49]. Fig. 1 shows the different types of the NSM bars used in this study. The mechanical properties of all NSM bars obtained from their manufacturers' datasheets are given in Table 2.

As previously mentioned, three commercially available filling materials were used in this study. The Renew Wrap NSM-Gel (NG) is a two-component high strength epoxy-based adhesive consisting of an epoxy resin and a hardener. This epoxy adhesive is specifically designed for NSM and other externally bonded (EB) strengthening applications. The Sikadur-30 (SD) is a two-component epoxy that consists of an epoxy resin and a filler. According to the manufacturer, the SD adhesive is

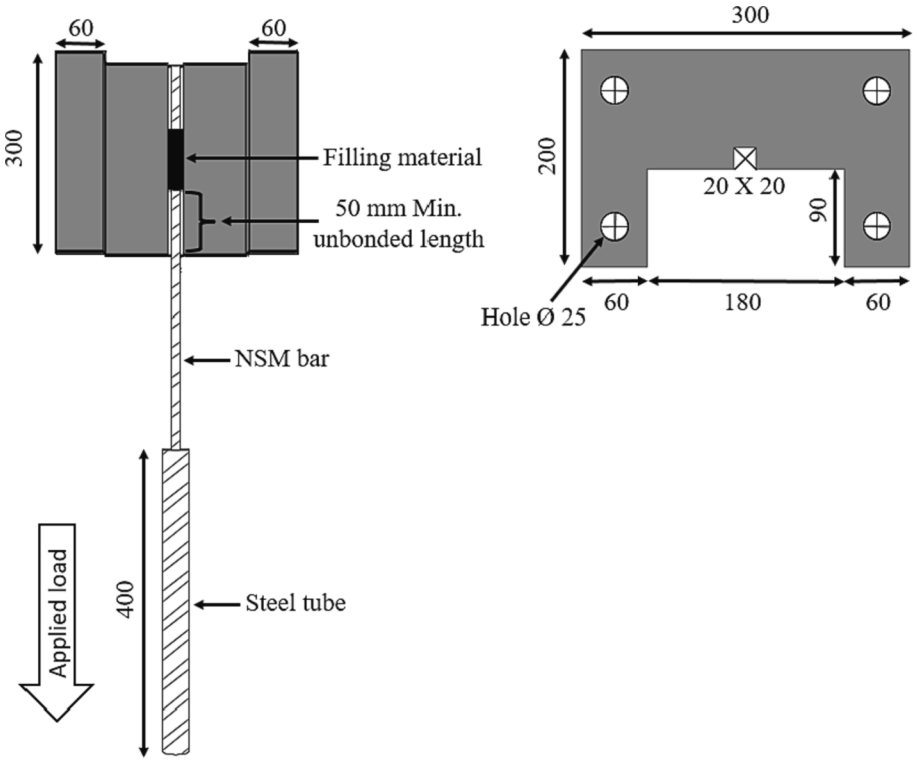

Fig. 2. A schematic view of the pullout test specimen (all dimensions are in *mm*).

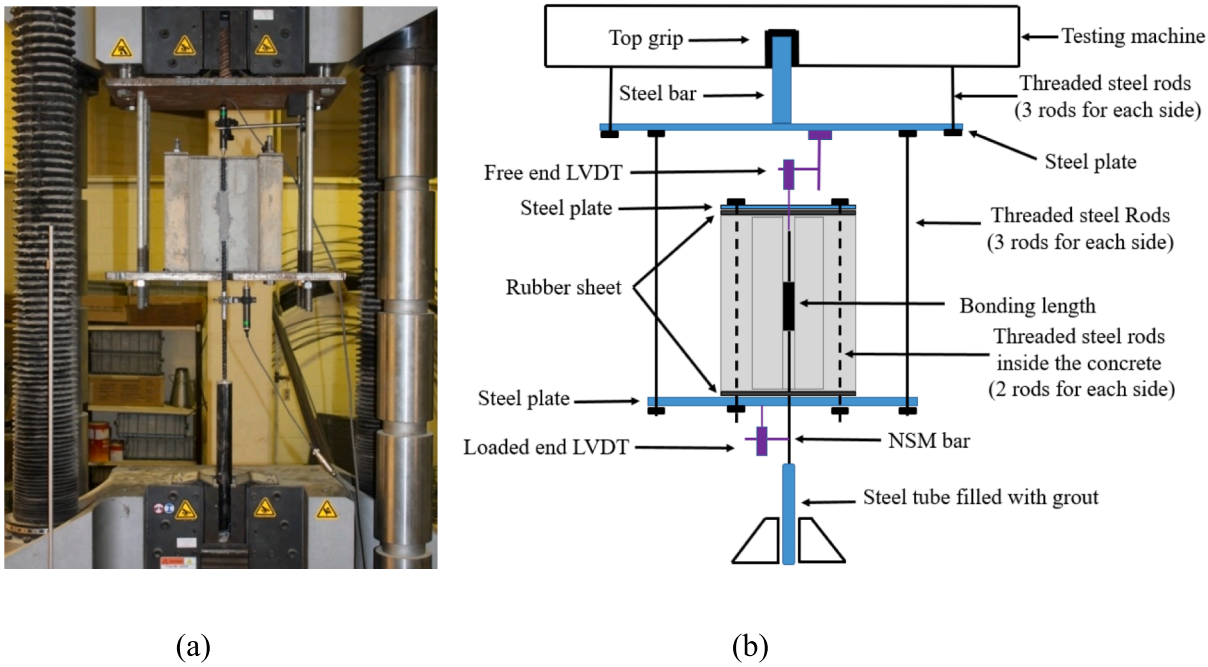

Fig. 3. (a) The test setup and (b) a schematic view of the pullout test setup.

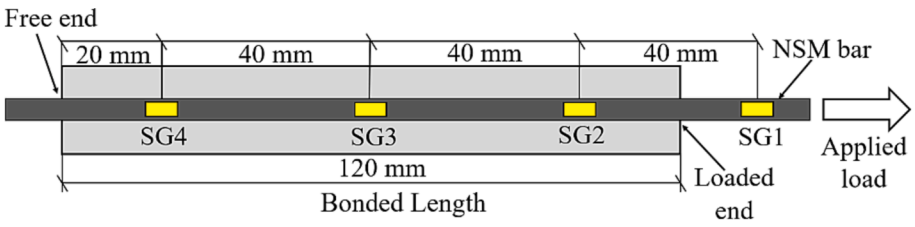

Fig. 4. Strain gauges installed on the deformed BFRP-NSM and SS-NSM specimens with bonded length of 12 d_b.

designed for general bonding and strengthening applications. On the other hand, the Sika grout-214 (SG) is a high precision non-shrink expanding grout. The material properties of each of those adhesives and grout are listed in Table 3.

2.2. Specimens' fabrication

The C-shaped concrete specimens were constructed as shown in Fig. 2. The outside dimensions of the specimens were 300 × 200 mm and the interior dimensions were 180 × 90 mm with a total height of 300 mm. The pullout specimens were cast in wooden molds. An electrical vibrator was used to ensure the consistency of the concrete mix during casting. The top surface of the concrete was then finished and covered with wet burlap. The specimens were left inside the laboratory for curing for 28 days to achieve the required compressive strength of concrete. Following the curing of concrete, a 20 mm square groove was carved along the center of each concrete specimen using a diamond blade saw. The groove size was chosen to meet the minimum size recommended by *ACI* 440.2R-17 [46] provisions of 1.5 d_b. The groove was then filled with the filling material to the required bonded length before inserting the NSM bar in the groove. Any excess material was removed, and the surface of the specimen was leveled. The reinforced specimens were kept in the laboratory for curing in accordance with manufacturer recommendations as shown in Table 3. The FRP bars were anchored with 400 mm long steel tubes with a diameter of 42.6 mm and a wall thickness of 4.85 mm filled with a cementitious grout in accordance with ASTM D7205-21 requirements [47]. All bars were extended 300 mm beyond the bottom surface of the concrete to provide adequate length for attaching the slippage measuring device. A minimum unbonded length of 50 mm was maintained in all specimens between the concrete surface near the loaded end and the onset of the bonded length to avoid stress concentration that may result at the corners of the groove (Fig. 2).

2.3. Test setup and instrumentation

The direct pullout tests were carried out using a 1500 kN Universal Testing Machine. As illustrated in Fig. 3, the specimens were attached to the machine by means of a steel frame that was fabricated using two steel plates of 30 mm thickness each, six threaded steel rods of 16 mm diameter each, and a vertical steel bar of 32 mm diameter. Another four threaded steel rods were installed in 25 mm holes that were pre-fabricated in the four corners of the concrete specimen. The rods were embedded in two stiffened plates placed on the upper and lower surfaces of the specimen to prevent the movement of the specimen during testing. Two rubber sheets were placed between the specimen's surface and the plates to distribute the applied force and to minimize the stress concentration on the specimen's surface.

Electrical strain gauges of 6 mm length were installed on the surface of the deformed BFRP and the SS bars in specimens having a bonded length 12 d_b to monitor the strain distribution along the bars during testing. Three strain gauges were placed within the bonded length and an additional strain gauge was applied in the unbonded region close to the loaded end as shown in Fig. 4.

All specimens were instrumented with two linear variable differential transducers (LVDTs) with a displacement capacity of 25 mm and accuracy of 0.001 mm to measure the bar slippage at both the free and

Table 4
Pullout test results.

Specimen	P_{max} (kN)	P_{max}/P_u (%)	$\tau_{avg,1}$ (MPa)	$\tau_{avg,2}$ (MPa)	$S_{max,\ le}$ (mm)	$S_{max,\ fe}$ (mm)	Failure Mode[b]
Deformed BFRP bars							
B-D-6-NG	35.4	40.6	18.8	9.8	2.3	1.4	*SEC*
B-D-12-NG[a]	44.8	51.5	11.9	6.2	2.4	1.6	*SEC*
B-D-24-NG	49.3	56.6	6.5	3.4	3.5	–	CT + *SEC*
B-D-6-SD	17.2	19.8	9.1	4.8	1.0	0.8	*SEC*
B-D-12-SD[a]	33.6	38.6	8.9	4.7	2.1	1.0	*SEC*
B-D-24-SD	41.7	47.9	5.5	2.9	2.2	1.2	CT + *SEC*
B-D-12-SG[a]	8.3	9.5	2.2	2.3	2.2	2.0	BGI
Sand-coated BFRP bars							
B-SC-6-NG	33.4	35.4	17.7	9.3	2.2	1.1	P-SD
B-SC-12-NG[a]	44.0	46.6	11.7	6.1	3.8	1.8	P-SD
B-SC-24-NG	49.9	52.8	6.6	3.5	3.3	1.4	CT + P-SD
B-SC-6-SD	31.7	33.5	16.8	8.8	2.0	0.8	P-SD
B-SC-12-SD[a]	37.1	39.4	9.9	5.2	2.4	1.1	P-SD
B-SC-24-SD	49.1	52.1	6.5	3.4	3.3	1.1	P-SD + CT
Deformed GFRP bars							
G-D-6-NG	26.8	24.3	14.2	7.4	1.0	0.8	*SEC*
G-D-12-NG[a]	42.7	38.7	11.3	5.9	2.4	1.7	*SEC*
G-D-24-NG	72.1	65.3	9.6	5.0	3.8	2.1	CS + *SEC*
G-D-6-SD	22.5	20.4	11.9	6.3	1.0	0.8	*SEC*
G-D-12-SD[a]	36.3	32.9	9.6	5.1	1.9	1.3	*SEC*
G-D-24-SD	54.2	49.1	7.2	3.8	2.2	1.9	CS + *SEC*
Sand-coated GFRP bars							
G-SC-6-NG	27.7	29.0	14.7	7.7	1.8	0.7	P-SD
G-SC-12-NG[a]	40.2	42.2	10.7	5.6	2.9	1.0	P-SD
G-SC-24-NG	59.3	64.8	8.2	4.3	4.2	1.3	CS + P-SD
G-SC-6-SD	21.8	22.8	11.5	6.0	1.5	0.6	P-SD
G-SC-12-SD[a]	39.2	41.1	10.4	5.5	2.9	1.1	P-SD
G-SC-24-SD	46.9	49.1	6.2	3.3	3.0	1.0	CS + P-SD
Deformed CFRP bars							
C-D-6-NG	39.6	28.5	21.0	11.0	1.1	1.1	CS + *SEC*
C-D-12-NG	52.9	38.1	14.0	7.4	3.2	2.8	CS + *SEC*
C-D-24-NG	53.9	38.8	7.2	3.7	3.7	1.0	CS + *SEC*
C-D-6-SD	36.7	26.4	19.5	10.2	1.5	1.2	CS + *SEC*
C-D-12-SD	48.8	35.2	13.0	6.8	2.1	2.7	CS + *SEC*
C-D-24-SD	54.4	39.2	7.2	3.8	1.8	0.8	CS + *SEC*
Deformed SS bars							
	17.1	37.3	9.1	4.7	1.2	–	*SEC*
SS-D-6-NG							
SS-D-12-NG[a]	35.2	76.6	9.3	4.9	1.8	1.0	*SEC*
SS-D-24-NG	45.8	99.7	6.1	3.2	1.3	1.1	CS + *SEC*
SS-D-6-SD	14.6	31.8	7.8	4.1	0.4	0.4	*SEC*
SS-D-12-SD[a]	27.8	60.5	7.4	3.9	2.0	1.1	*SEC*
SS-D-24-SD	39.1	85.1	5.2	2.7	1.5	0.7	CS + *SEC*
SS-D-12-SG[a]	6.3	13.6	1.7	0.9	1.5	1.4	BGI

[a] Average results of three tested replicates.
[b] *SEC* = splitting of the epoxy cover; P-SD = bar pullout and surface delamination; CS = concrete splitting; BGI = failure at bar-grout interface.

loaded ends. The pullout specimens were tested under displacement control at a rate of 0.2 mm/min up to failure. Readings from the load cell, the LVDTs, and the strain gauges were collected using an automatic data acquisition system.

3. Experimental results and discussion

Table 4 summarizes the test results in terms of the maximum pullout load, P_{max}, the load efficiency factor, $P_{max}/P_{u,}$ where P_u is the ultimate tensile force of the NSM bar as reported by the manufacturer, the maximum slip at both the loaded and free ends, $S_{max.\ le}$ and $S_{max.\ fe}$, respectively, which corresponds to the maximum pullout load, P_{max}, and the mode of failure of the tested specimens. Two values for the bond strengths are also reported in Table 4 namely, (a) the average bond strength of the bar, $\tau_{avg,1}$, which defines the bond strength between the bar and the surrounding adhesive as determined at the bar-adhesive interface at failure and (b) the average bond strength between the NSM system (the bar and the adhesive) and the surrounding concrete, $\tau_{avg,2}$, as determined at the concrete-adhesive interface at failure. The bond strengths $\tau_{avg,1}$ and $\tau_{avg,2}$ were calculated using Equations (1) and (2), respectively, as follows:

$$\tau_{avg,1} = \frac{P_{max}}{\pi d_b L_b} \tag{1}$$

$$\tau_{avg,2} = \frac{P_{max}}{(a+2b)L_b} \tag{2}$$

where L_b is the bonded length and a and b are the width and depth of the rectangular groove, respectively. In the current specimens, a and b were 20 mm each.

3.1. Failure modes

As listed in Table 4, four modes of failure were observed throughout the tests as follows:

(a) splitting of the epoxy cover (*SEC*)

This mode of failure characterized all the tested specimens with deformed NSM bars of short and medium bonded lengths (6 d_b and 12 d_b, respectively) that were adhered to concrete using the NG and SD epoxy adhesives. Those specimens failed by splitting of the epoxy cover around the NSM bar. Failure was accompanied by the detachment of a thin layer of concrete along the bonded length of the NSM bar as shown in Fig. 5 for specimens B-D-12-NG and B-D-12-SD. This mode of failure was sudden and explosive in nature as the specimen approached its peak load. In most of the tested specimens that failed due to *SEC*, splitting

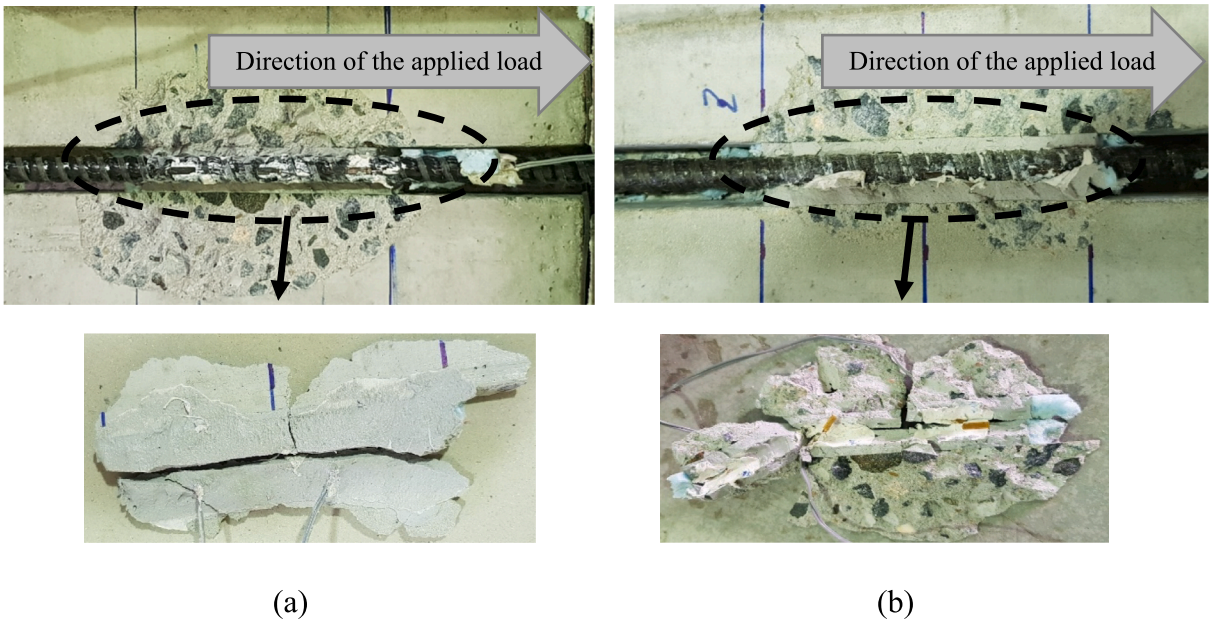

Fig. 5. Splitting of the epoxy cover (*SEC*) in specimens: (a) B-D-12-NG and (b) B-D-12-SD.

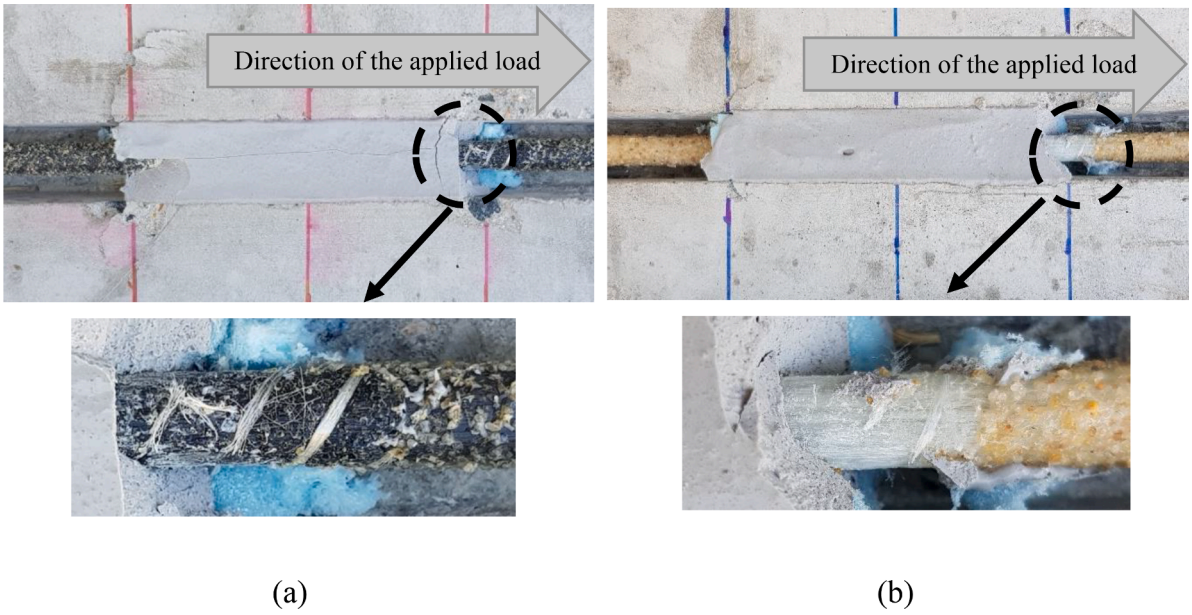

Fig. 6. Bar surface delamination in specimens: (a) B-SC-12-NG and (b) G-SC-12-NG.

started at the loaded end and propagated towards the free end of the specimen. It is worth noting that the epoxy's bottom and side surfaces remained intact with the concrete after failure indicating a perfect bond between the adhesive and the concrete. The NSM bar also remained intact with the bottom layer of the epoxy adhesive.

(b) bar pullout and surface delamination (P-SD)

This mode of failure characterized all sand-coated BFRP and GRFP bars with short and medium bonded lengths (6 d_b and 12 d_b, respectively) that were adhered to concrete using the NG and SD epoxy adhesives. The outer layer of the bar (the sand-coated layer) was peeled off at the end of testing revealing the original color of the polymers in both the BFRP and GFRP bars as can be depicted in Fig. 6 for specimens B-SC-12-NG and G-SC-12-NG. The surface of the bar was obviously damaged at the loaded ends of the bars. Upon examining the failed specimens, no traces of epoxy were found on the surface of the bar indicating a local mode of failure that was governed by the shear stresses between the outer layer of the bar and its subsequent layers after being pulled out from the adhesive. This mode a failure is common in sand-coated bars as reported in previous studies [27,51].

(c) concrete splitting (CS)

This mode of failure characterized all specimens with bonded lengths of 24 d_b (due to the long-bonded region embedded within the concrete) in addition to all specimens reinforced with CFRP bars (due to their high tensile strength). A longitudinal crack was observed along the concrete specimen at peak loads as shown in Fig. 7 for specimens B-D-24-SD, B-SC-24-NG, and C-D-24-NG. The crack initiated longitudinally at the loaded end and propagated towards the free end along the center of the groove causing splitting of the specimen. This mode of failure was obviously governed by the concrete strength rather than the tensile strength of the bar or the shear stresses along the epoxy-concrete and the

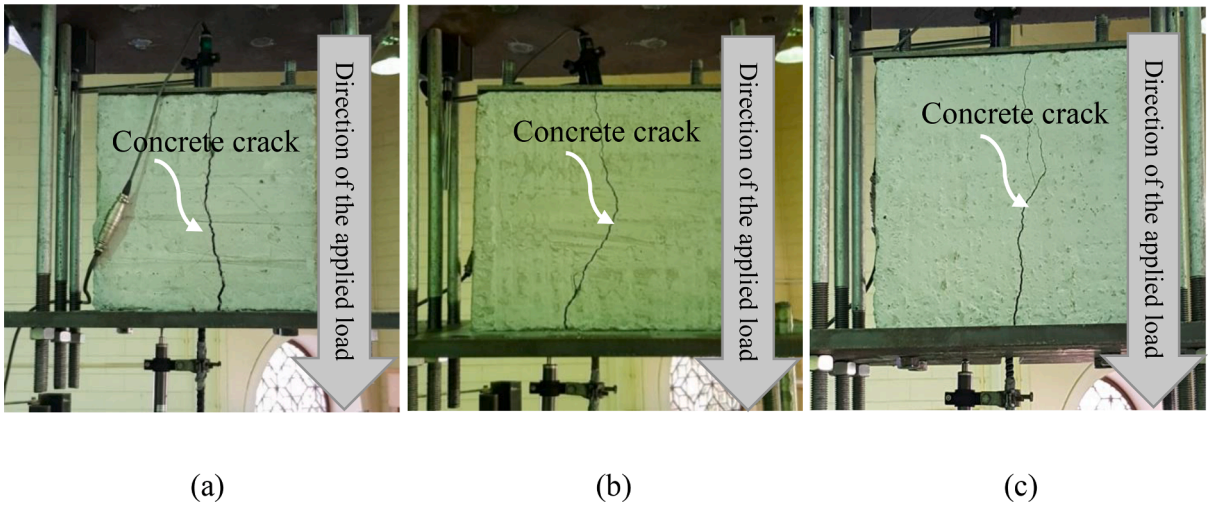

Fig. 7. Concrete splitting in specimens: (a) B-D-24-SD, (b) B-SC-24-NG, and (c) C-D-24-NG.

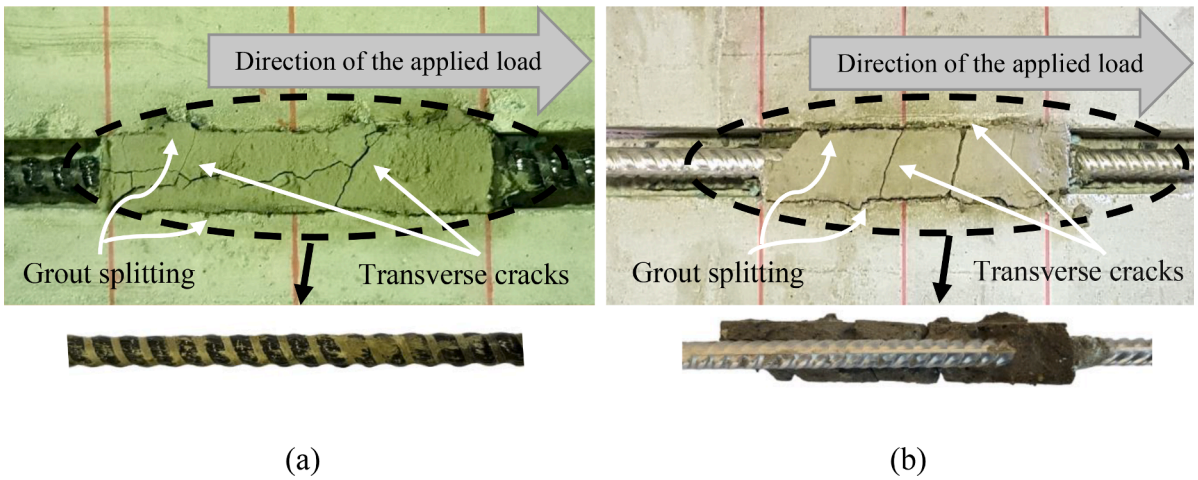

Fig. 8. Failure at the bar-grout interface in specimens: (a) B-D-12-SG and (b) SS-D-12-SG.

epoxy-NSM bar interfaces. It should be mentioned that this failure was brittle and sudden with no prior indication of cracking was observed on the concrete surface.

(d) Bar-grout interface (BGI)

This mode of failure characterized all specimens with NSM bars that were bonded using Sika grout-214. Failure of those specimens occurred by debonding of the NSM bar at the bar-grout interface at loading levels well below those encountered in the epoxy-bonded specimens, as will be detailed later. This mode of failure was attributed to the low tensile strength of the grout material compared to that of the epoxy adhesives. As the applied load increased during testing, several transverse cracks were formed in the grout at the loaded end of the bars and propagated towards their free end as shown in Fig. 8 for specimens B-D-12-SG and SS-D-12-SG.

3.2. Bond stress-slip response

The relationships between the average bond stress at the bar-adhesive interface and the slippage measured at the free end of the pullout specimens are shown in Fig. 9. All bond stress-slip curves showed a linear ascending branch up to the peak bond stress, $\tau_{max.}$ At the onset of loading, slippage of all bars was nil and increased as the applied load increased to about 50 to 60 % of the peak stress with no observation of cracks in the epoxy or the concrete. Beyond this load, explosive sounds were noted indicating the formation of cracks in the adhesive cover and/or the concrete surrounding the groove. Further increase in the applied load resulted in more visible cracks that propagated longitudinally in the adhesive towards the free end of the NSM bar and more slippage between the bar and the surrounding adhesive was noticed.

Fig. 9 shows representative bond stress-slip curves illustrating the effect of the various parameters on the bond behavior of the tested specimens. Fig. 9 (a) shows the bond stress-slip response of the BFRP bars adhered to concrete with the three types of adhesives used. After reaching the peak stress, the bond stress-slip curves of specimens adhered with epoxy-based adhesives (NG and SD adhesives) showed a sudden descending branch that was characterized by a significant decrease in the bond stress accompanied by a large increase in the bar slippage. This abrupt loss of bond explained the explosive sound when the specimens reached their peak load, which was attributed to the splitting of the epoxy adhesive. Specimens adhered with the cementitious grout (SG) showed a more ductile behavior as shown in Fig. 9 (a) for the BFRP specimens. Fig. 9 (a) also demonstrates the superiority of the epoxy-based NG adhesive over the SD and SG adhesives. It can be observed that specimen B-D-12-NG showed higher bond strength and larger slippage at its free end than its counterparts adhered with the SD and SG adhesives. This finding was attributed to the high shear strength of the NG adhesive, which enabled the specimens to sustain large pullout forces.

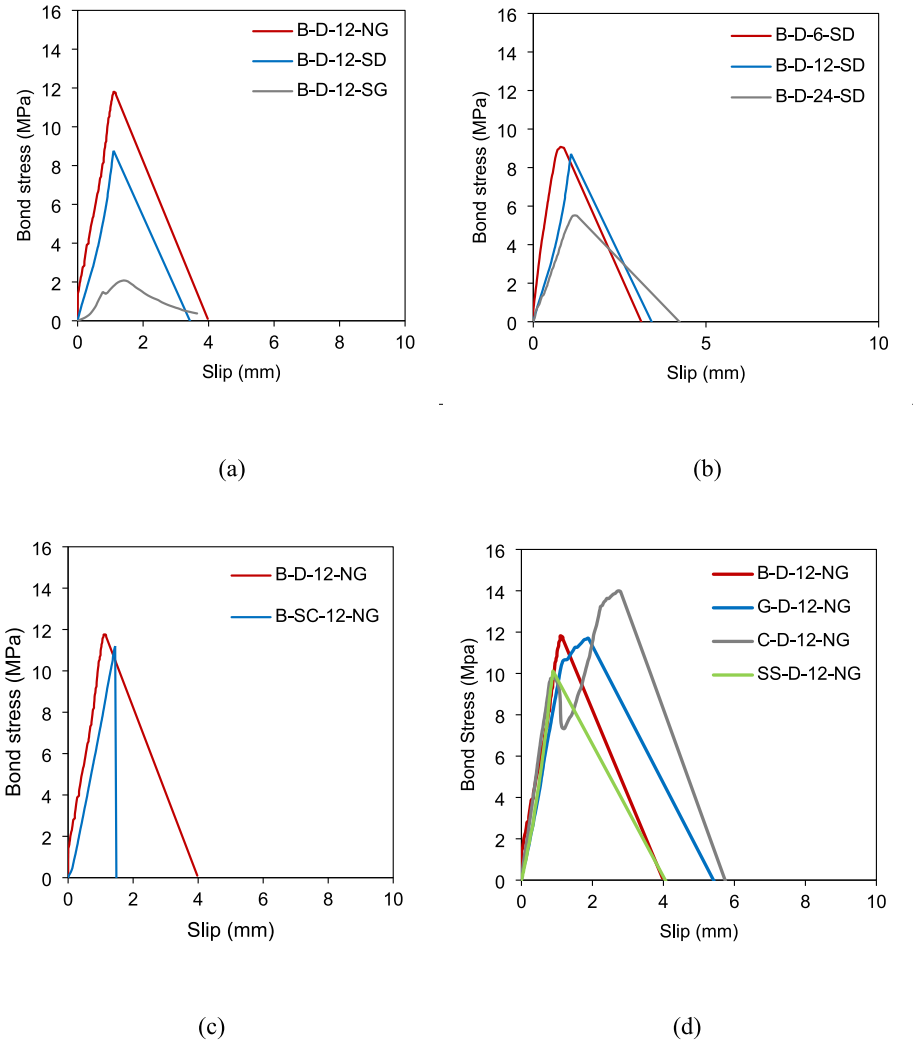

Fig. 9. Bond stress-slip curves of representative pullout specimens.

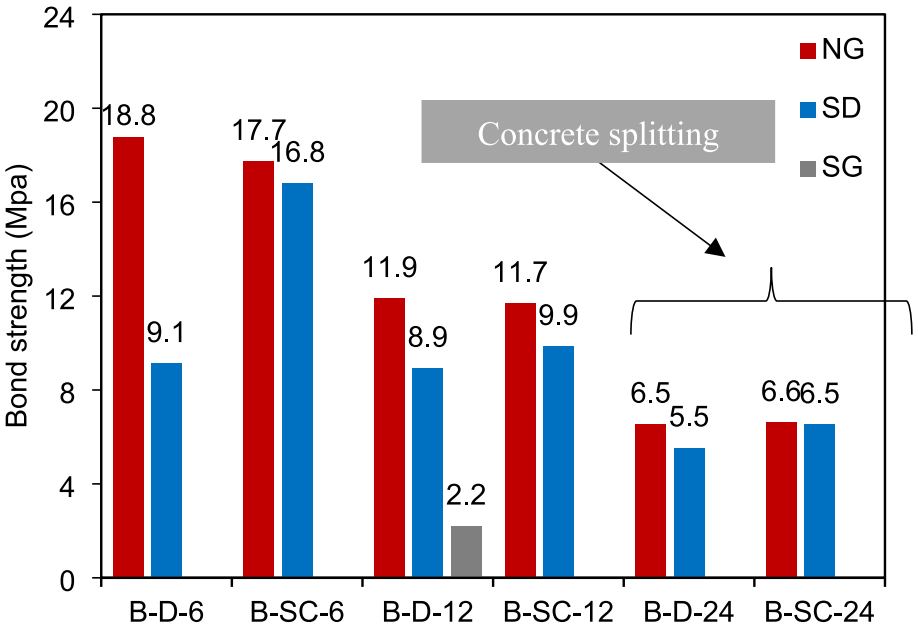

(a) BFRP Bars

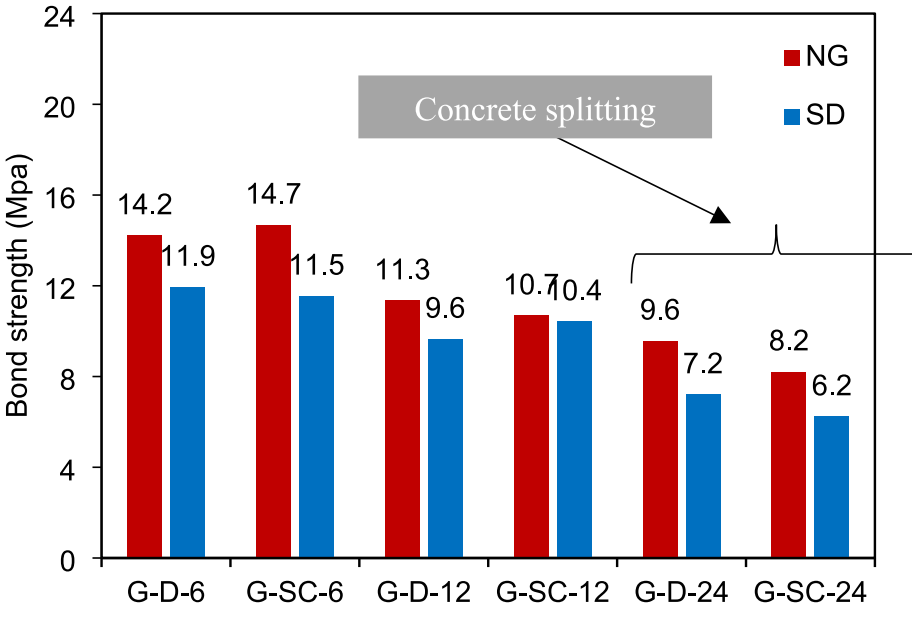

(b) GFRP Bars

Fig. 10. Effect of the type of epoxy adhesives used on the bond strength of the NSM bars.

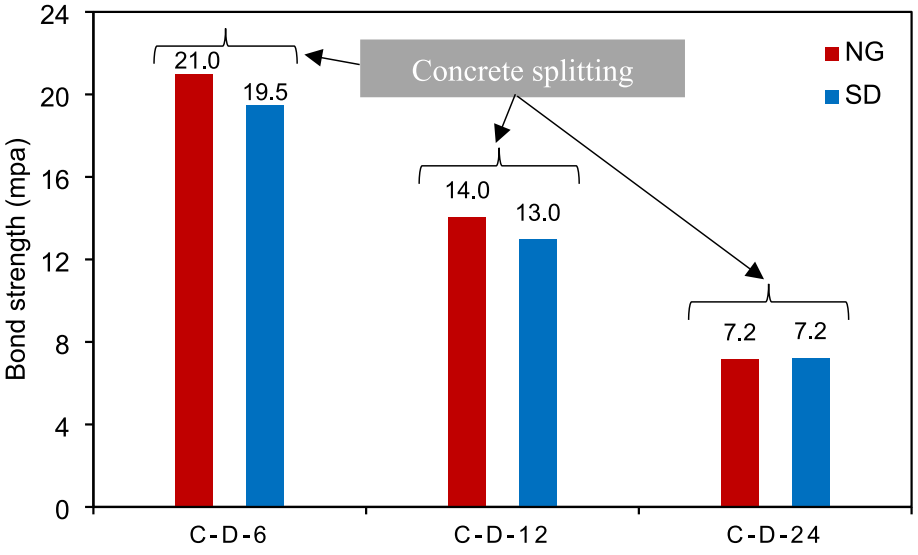

(c) CFRP Bars

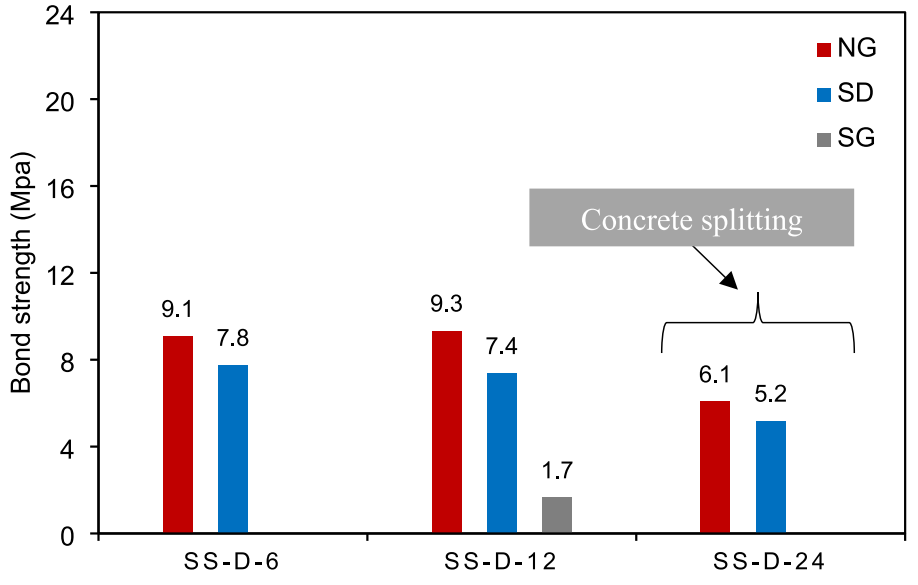

(d) SS Bars

Fig. 10. (*continued*).

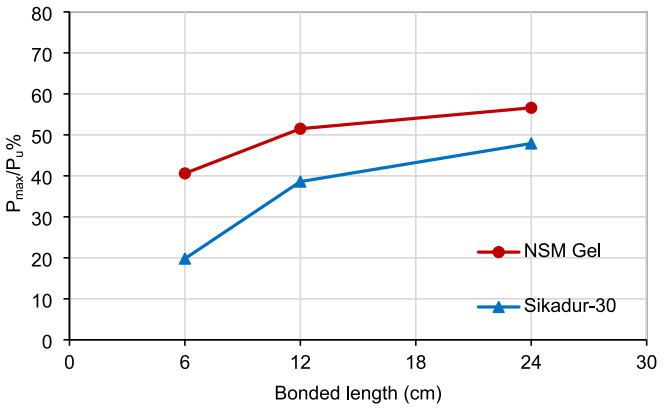

Fig. 11. Variation of the load efficiency ratio, P_{max}/P_u (%) with the epoxy-based adhesives.

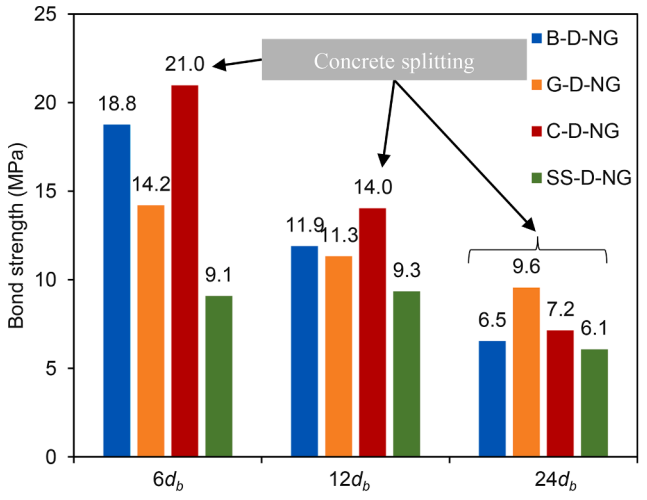

(a)

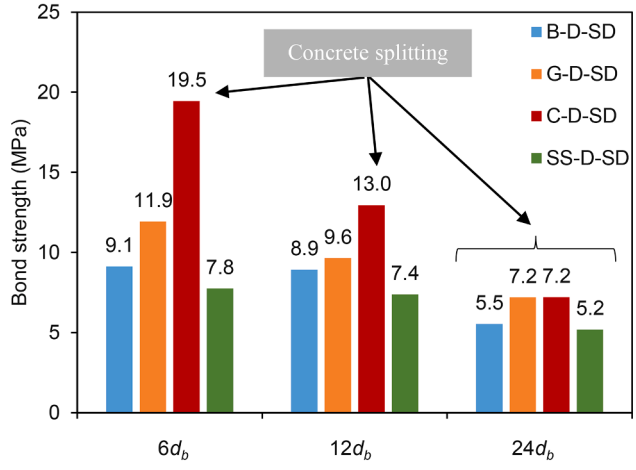

(b)

Fig. 12. Bond strength of different types of deformed NSM bars inserted in (a) NG and (b) SD epoxy adhesives.

Specimens with different bonded lengths demonstrated similar trends as shown in Fig. 9 (b) for specimens B-D-6-SD, B-D-12-SD, and B-D-24-SD. As the bonded length increased, the bond stress decreased due to the non-uniform distribution of stresses along the bonded length of the bar. These results confirmed the findings reported in previous studies [16,52,53].

The effect of the bar material and its surface texture on the bond stress-slip response of the tested specimens can be depicted in Fig. 9 (c) and (d), respectively. No obvious variation in the observed trend can be confirmed from the obtained data since all specimens showed similar ascending and descending branches. The only exception to this trend was for specimen C-D-12-NG that showed two peaks during testing as shown in Fig. 9 (d). This behavior was attributed to the high strength of both the CFRP bar and the NG adhesive. The specimen was able to restore its capacity after the first peak to attain a higher peak load as shown in Fig. 9 (d).

4. Factors affecting the bond strength of the NSM bars

4.1. The adhesive material

Fig. 10 shows the bond strengths developed in the tested specimens when different types of adhesives were used. As a general trend, the NG adhesive outperformed the other adhesives in developing the bond strength of almost all the tested specimens regardless of the bar material followed by the SD and the SG adhesives. As previously mentioned, the NG and SD epoxy adhesives outperformed the cement grout and allowed the specimens to withstand higher bond strengths. For instance, the bond strength of specimens B-D-12-NG and B-D-12-SD were 11.9, and 8.9 MPa respectively, whereas the bond strength of specimens B-D-12-SG was 2.2 MPa. These findings were consistent with those reported by Wang et al. [25]and Soliman et al. [19] who concluded that epoxy adhesives allowed specimens to withstand higher stresses than the cementitious mortars before failure owing to their high bonding strength.

It was also observed that the developed bond strength in the NSM bars was directly proportional to the shear strength of the adhesive listed in Table 3. For instance, the bond strength developed in the BFRP bars adhered with the NG adhesive revealed an increase between 33 and 108 % compared to their counterparts adhered with the SD adhesive for bonded lengths of 6 d_b and 12 d_b, respectively. A similar trend was observed in the GFRP- and SS-NSM bars as illustrated in Fig. 10 (b) and (d), respectively. For instance, the bond strength of the NSM-SS bars adhered with the NG adhesive increased by 16.7 and 25.7 % as compared to those adhered with the SD adhesive for bonded lengths of 6 d_b and 12 d_b, respectively. Those results were confirmed by plotting the variation of the load efficiency ratio, P_{max}/P_u, with the epoxy-based adhesive used in Fig. 11 for the deformed BFRP bars. It can be observed that the BFRP bars adhered with the NG adhesive showed higher bond strength than those adhered with the SD adhesive regardless of the bonded length used. On the other hand, the influence of the adhesive type was marginal for the CFRP specimens and those with bonded length of 24 d_b since their failure was governed by the concrete rather than the NSM system as can be depicted from Fig. 10(c).

4.2. The NSM bar material

Fig. 12 compares between the bond strengths of the different types of the NSM bars having different bonded lengths. Recall that all bars with bonded length of 24 d_b failed due to concrete splitting and therefore, were excluded from this analysis (also shown in the plots for convenience).

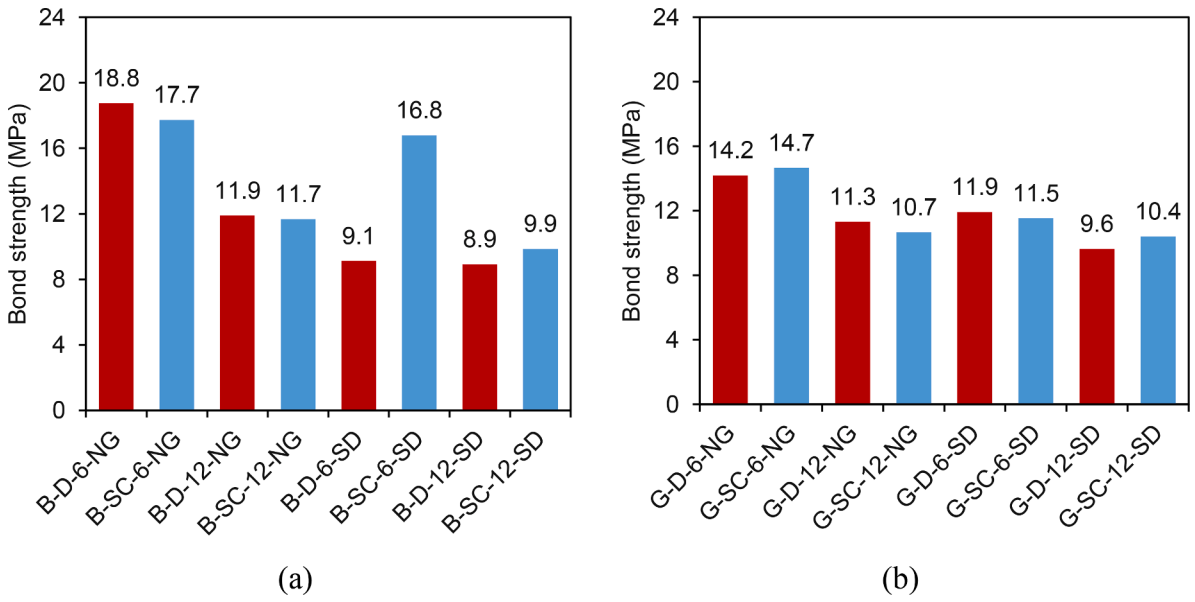

Fig. 13. Effect of the texture of the NSM bars on their bond strength: (a) specimens with BFRP bars and (b) specimens with GFRP bars.

The CFRP bars consistently recorded the highest bond strength among all other bars regardless of their bonded lengths and the adhesive material used. For instance, specimen C-D-12-NG (bonded with the NG adhesive with a bonded length of 12 d_b) showed a bond strength of 14 MPa, which was 18, 24, and 50 % higher than that of specimens B-D-12-NG, G-D-12-NG, and SS-D-12-NG, respectively. Similarly, the bond strength of specimen C-D-12-SD (bonded with the SG adhesive with a bonded length of 12 d_b) was 13 MPa, which was 45, 34, and 75 % higher than that of specimens B-D-12-SD, G-D-12-SD, and SS-D-12-SD, respectively. These findings was attributed to the high tensile strength of the CFRP bar as compared to other bars' materials, allowing the specimens to resist higher loads prior to failure. They also confirmed the observed mode of failure of the CFRP specimens by concrete splitting.

On the other hand, the deformed BFRP and GFRP bars with bonded length of 12 d_b showed almost similar bond strengths as can be depicted in Fig. 12. Specimens B-D-12-NG and G-D-12-NG showed average bond strengths of 11.9 and 11.3 MPa, respectively, whereas specimens B-D-12-SD and G-D-12-SD showed average bond strengths of 9 and 9.6 MPa, respectively. On the other hand, the SS bars showed the least bond strength among the tested bars with bond strengths of 9.3 and 7.4 MPa for specimens SS-D-12-NG and SS-D-12-SD, respectively. This finding was confirmed with the mode of failure observed in the SS specimens, which occurred due to splitting of the epoxy cover around the bars. The lower strength of the SS bars and the associated mode of failure observed during the tests were attributed to the stiffer and more pronounced ribs of the SS bars as compared to those of the FRP bars, which might have caused the epoxy adhesive to fracture around the bars at lower pullout loads.

4.3. The bar texture

The bar texture is a critical parameter that defines the bond behavior of the NSM bar and directly affects the stress transfer between the bar and the surrounding adhesive through frictional and mechanical interlocking mechanisms [18]. The current experimental results revealed that the bar texture also governed the mode of failure of the tested specimens. As previously mentioned in Table 4, all deformed FRP bars adhered with epoxy adhesives failed due to splitting of their epoxy cover regardless of their bar material. The deformed texture played a major role in developing the mechanical interlocking between the bar and the surrounding adhesive, which allowed the specimens to develop their distinct bond strengths. On the other hand, the sand-coated BFRP and GFRP bars failed due to the delamination of the external sanded layer of the FRP bar when the bar was pulled out. The fact that the epoxy adhesive surrounding the bar and the concrete along the bonded length remained undamaged suggested that the bond strength of the sand-coated bars was developed primarily by adhesion and friction.

Nevertheless, the test results revealed that the bar texture had a slight effect on the bond strength of the tested bars. This finding can be depicted from the results shown in Fig. 13. Apart from specimen B-SC-6-SD, both deformed and sand-coated BFRP bars showed almost similar bond strengths. For instance, specimens B-D-12-NG and B-SC-12-NG showed bond strengths of 11.9 and 11.7 MPa, respectively, as shown in Fig. 13 (a) whereas specimens G-D-12-NG and G-SC-12-NG encountered bond strengths of 11.3 and 10.7 MPa, respectively, as shown in Fig. 13 (b).

The test results also suggested that the bar texture should not be recognized as the sole factor that affected the bond performance of the NSM-FRP bars. Nonetheless, it must be weighed collectively with other factors such as the bonded length and the material of the tested bar in addition to the adhesive used.

4.4. The bonded length

Fig. 14 compares between the bond strengths obtained for the tested NSM bars having different bonded lengths of 6 d_b, 12 d_b, and 24 d_b. The test results showed that the bond strength of the NSM bars was inversely proportional to their bonded length, which was attributed to the larger contact area between the NSM bar and the surrounding adhesive when the bonded length of the bar increased, as can be depicted from Eq. (1). As the bonded length increases, the bond stress is unevenly distributed throughout the bonded portion of the bar, thus reducing its bonded strength [16,27,52–55]. This finding was valid for all NSM bars regardless of the adhesive used and was more pronounced in FRP bars rather than in SS bars. It is worth noting that the SS bars lost their bond resistance in a more abrupt manner than their FRP counterparts. As previously explained, the stiff and pronounced ribs of the SS bars have caused the fracture of the surrounding epoxy, which occurred in an

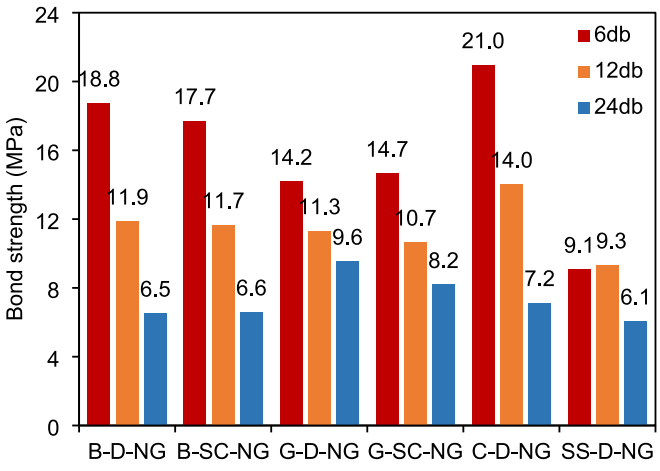

(a) NSM gel (NG) epoxy adhesive

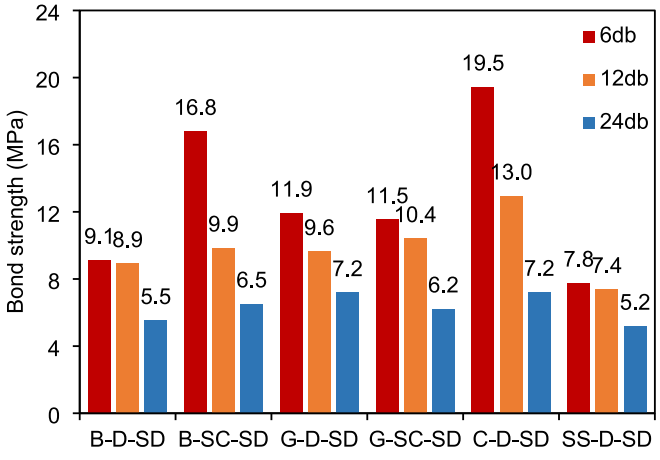

(b) Sikadur–30 (SD) epoxy adhesive

Fig. 14. Variation of the bond strength of the tested NSM bars with their bonded length.

abrupt and explosive manner.

It can be noticed that the effect of the bonded length on the strength of the NSM bars was more pronounced in the deformed BFRP bars than in the deformed GFRP bars when the NG adhesive was used. For instance, the bond strengths of specimens B-D-NG decreased by 37 and 45 % when their bonded lengths increased from 6 d_b to 12 d_b and 24 d_b, respectively, compared to only 20 and 15 % decrease in the bond strength of of specimens G-D-NG for the same bonded lengths. This finding can be attributed to the distinct shape of the ribs that characterized the surface of the BFRP bars as shown in Fig. 1, which ensured an excellent interlocking mechanism of the BFRP bars as will be explained later.

A similar trend was also noticed by comparing the bond strengths of the sand-coated BFRP and GFRP bars. The bond strengths of specimens B-SC-NG decreased by 34 and 44 % when their bonded lengths increased from 6 d_b to 12 d_b and 24 d_b, respectively, compared to 27 and 23 % decrease in the bond strength of specimens G-SC-NG bars for the same bonded lengths. These results indicated the better quality of the sand-coated layer of the BFRP bars used in this study as compared to the GFRP bars. In fact, it was observed that the sand particles of the BFRP bars were larger and better distributed on the bar's surface than those of the GFRP bars. This high quality of the sand-coated layer of the BFRP bars allowed the epoxy adhesive to enter between the sand particles, which improved the mechanical interlocking between the bar and the adhesive, leading to higher bond strength as compared to the GFRP bars.

5. Strain distribution

Data from the strain gauges were utilized to plot the strain distribution along the bonded length of the NSM bars. Fig. 15 shows the strain distribution profiles along the BFRP and SS bars for specimens B-D-12-NG and SS-D-12-NG, as representative specimens, at different percentages of the specimens' peak pull-out load, P_{max}.

At low levels of the applied loads, the strains along the NSM-BFRP bars were almost nil at their free ends and increased gradually at their loaded ends. At this stage, the NSM-BFRP bars exerted tensile stresses on the surrounding adhesive and the chemical adhesion between the bar and the adhesive governed the bond mechanism. As the loading progressed, the chemical adhesion between the NSM-BFRP bars and the adhesive was gradually lost and the interfacial slip initiated, which resulted in a uniform increase in the recorded strains along the bar. At this stage, the mechanical interlocking between the bar and the adhesive was the only resisting mechanism and was greatly affected by the surface configuration of the bars and the adhesive used, as previously discussed.

On the other hand, the strains recorded in the SS bars increased suddenly as the load increased, unlike the gradual increase in the BFRP bars, until the specimen failed. This finding might be attributed to the distinct bond mechanisms of the two materials. As previously mentioned, the chemical adhesion between the BFRP bar and the adhesive governed the bond mechanism at early stages of loading. In SS bars, the bond between the bars and the surrounding adhesive was mainly governed by the mechanical interlocking due to the presence of lugs on their surfaces. Therefore, as the applied load increased, the adhesive surrounding the lugs was crushed and a sudden slippage occurred at each increment of the applied load, which was reflected as sudden increases in the strains recorded in the SS bars. The strain profile of the SS bars agreed well with their bond-slip curve obtained. The measured strains were generally smaller in the SS bars than in the BFRP bars due to the higher modulus of the former bars.

6. SEM observations

A scanning electron microscope (SEM) was used to examine the failed deformed BFRP, GFRP, and CFRP specimens (B-D-12-NG, B-D-12-SD, G-D-12-SD, and C-D-12-NG) and the failed sand-coated BFRP and GFRP specimens (B-SC-12-NG, B-SC-12-SD, and G-SC-12-SD). All specimens were cut at the middle of their bonded length through the NSM bar to examine the damage at the bar-epoxy interface. All samples were polished and coated with a thin layer of gold before being scanned. The prepared samples were then scanned with a NOVA NANOSEM 450 machine.

The SEM images for the deformed specimens B-D-12-NG, B-D-12-SD, G-D-12-SD and C-D-12-NG are shown in Fig. 16 (a) to (d). The enclosed areas shown on the SEM images designate the bar-adhesive interface in all the examined specimens. As can be depicted from the images, no empty gaps could be observed at the bar-adhesive interface in any of the deformed specimens, which suggested an excellent adhesion between the NSM bar and the surrounding epoxy adhesive. Recall that those specimens failed due to splitting of the epoxy cover in the BFRP and GFRP specimens and due to concrete splitting in the CFRP specimen.

Fig. 16(e) to (g) show the SEM images of the sand-coated specimens B-SC-12-NG, B-SC-12-SD, and G-SC-12-SD. A visible gap between the sand-coated bars and the surrounding epoxy adhesive could be observed indicating the bar delamination from the adhesive prior to failure, which

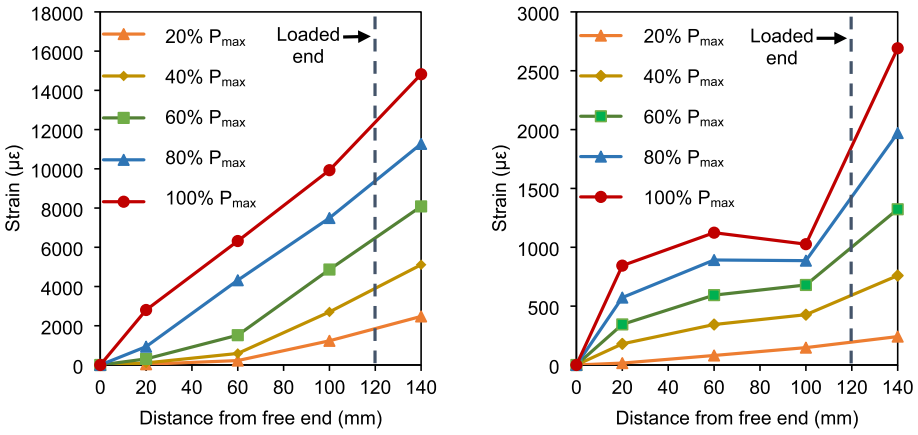

Fig. 15. Strain distribution in specimens (a) B-D-12-NG and (b) SS-D-12-NG.

agreed well with the mode of failure of the above mentioned specimens.

7. Theoretical analysis

The BPE model, previously developed by [56] to describe the bond-slip relationship for deformed steel bars, was implemented to model the ascending branch of the bond-slip curve of the NSM-FRP bars. Previous studies calibrated the model for CFRP and GFRP bars [55,57] and more recently for the BFRP bars [27,58]. The BPE model describes the ascending branch of the bond-slip relationship as follows:

$$\tau(s) = \tau_{max} \cdot \left(\frac{S}{S_{max}}\right)^{\alpha} for 0 \le S \le S_{max} \quad (3)$$

Where τ and s are the bond stress and the corresponding slip at any stage of loading, respectively, while τ_{max} and s_{max} are their corresponding maximum values. The parameter α is a curve fitting parameter calibrated from the experimental data by equating the area underneath the experimental and analytical ascending branches of the experimental and analytical bond-slip curves as per Equation (4) within a tolerance margin.

$$A_{\tau 1} = \int_0^{Smax} \tau_{max}\left(\frac{S}{S_{max}}\right)^{\alpha} d_s = \frac{\tau_{max} S_{max}}{1+\alpha} \quad (4)$$

Therefore, α can be expressed as a function of $A_{\tau 1}$ as follows:

$$\alpha = \frac{\tau_{max} \cdot S_{max}}{A_{\tau 1}} - 1 \quad (5)$$

The parameter α should be less than 1 to be meaningful. It varies with the characteristics of the FRP bar under study and the properties of the concrete/adhesive that surrounds the bar. Cosenza et al. [59] reported that the indented, sand-coated, and ribbed FRP bars surrounded by concrete had average values for of 0.177, 0.067, and 0.283, respectively. In this study, was determined using curve fitting of the experimental data obtained at the unloaded ends rather than at the loaded ends. This agreed well with the design requirements of FRP-reinforced structures that no slip should occur at the unloaded ends of the FRP bars under the applied service loads [27,60].

The average values of the fitting parameter α for all the examined FRP bars are listed in Table 5. The obtained results suggested that α ranged between 0.92 and 0.95 for the deformed BFRP bars and between 0.77 and 0.80 for the sand-coated BFRP ones. This discrepancy in the values of α within the specimens having the same surface texture can be attributed to the type of the adhesive used, which affects the bond behavior of the tested bars and therefore, their bond-slip relationship. Similarly, the parameter α for the deformed GFRP bars ranged between 0.70 and 0.75, which was considerably less than the values encountered in the deformed BFRP bars. This variation can be explained by the different surface texture of both types of bars as shown in Fig. 1. On the other hand, the sand-coated GFRP bars showed values of α that ranged between 0.91 and 0.93, respectively, which were higher than those of the sand-coated BFRP bars indicating a stiffer bond stress-slip relationship for the BFRP bars than the GFRP bars as can be depicted from Fig. 9 (d). Finally, the steep bond stress-slip behavior of the deformed CFRP bars was reflected in the values of α obtained for those bars, which ranged between 0.53 and 0.49. Those low values of α characterized the steep ascending branch of the NSM-CFRP bars as observed during the tests and indicated the high initial stiffness of the CFRP bars at this stage of loading. Fig. 17 shows a comparison between the analytical curves obtained using the BPE model and the experimental results for representative NSM-BFRP and GFRP bars. Good correlation between the analytical and experimental curves is observed.

8. Conclusions

In this study, sixty-six C-shape concrete pull-out specimens were constructed and tested in direct pullout tests to investigate the bond performance of NSM bars. The parameters investigated included the bar types, the bar surface configuration, the bonded length, and the filling adhesives. Based on the test results, the following conclusions can be drawn:

1- The deformed NSM-BFRP and GFRP specimens with short and medium bonded lengths (6 d_b and 12 d_b) failed due to splitting of the epoxy cover with no indication of distress at the concrete-adhesive interface whereas their sand-coated counterparts failed due to the delamination of the outer sand-coated layer.
2- Specimens with bonded length of 24 d_b and all NSM-CFRP specimens failed due to concrete splitting during testing. This mode of failure was brittle and sudden with no prior indication of cracking was observed on the concrete surface.
3- Specimens filled with the cementitious grout showed the least bond strength among all other specimens. Failure of those specimens occurred due to debonding of the NSM bar at the bar-grout interface

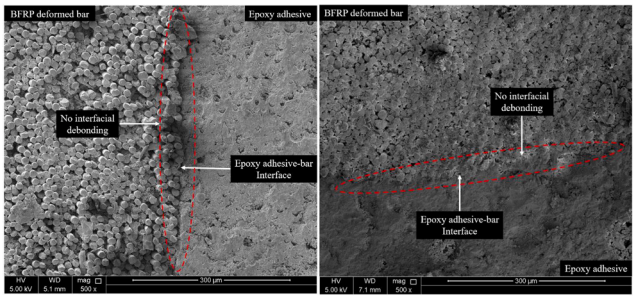

(a) B-D-12-NG (b) B-D-12-SD

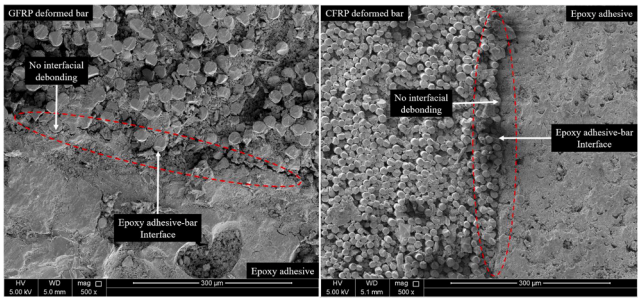

(c) G-D-12-SD (d) C-D-12-NG

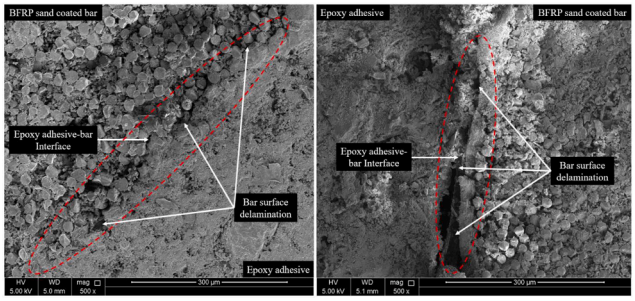

(e) B-SC-12-NG (f) B-SC-12-SD

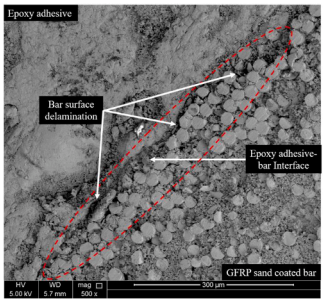

(g) G-SC-12-SD

Fig. 16. SEM images for (a to d) the deformed and (e to g) sand-coated specimens at the bar-adhesive interface.

at loading levels well below those encountered in the epoxy-bonded specimens.

4- The shear strength of the adhesive material had a significant influence on the bond strength of the NSM bars. The NG epoxy adhesive outperformed the other adhesives in developing the bond strength of almost all the tested specimens regardless of their bar material followed by the SD and the SG adhesives.
5- Increasing the bonded length of all NSM specimens resulted in a considerable increase in the maximum pullout loads. The average bond strength developed decreased as the embedded length of the NSM bar increased due to the non-uniform bond stress distribution along the embedded length.
6- Both the deformed and sand-coated NSM-BFRP and GFRP bars showed almost similar bond strengths. The bar texture investigated in this study had a slight effect on the developed bond strength of the tested bars. The NSM-CFRP bars showed the highest bond strength as compared to their BFRP, GFRP, and SS counterparts.
7- The BPE model can be used to describe the bond-slip relationship for the NSM-FRP bars investigated in this study. The parameter α can be taken as 0.935 and 0.785 for the deformed and sand-coated NSM-BFRP bars, respectively, and 0.725 and 0.92 for the deformed and sand-coated NSM-GFRP bars, respectively. A conservative value of 0.51 can best describe the performance of the deformed NSM-CFRP bars.

Table 5
Proposed fitting parameter α as obtained from the experimental results.

Specimen ID	α
BFRP specimens	
B-D-12-NG	0.92
B-D-12-SD	0.95
B-SC-12-NG	0.77
B-SC-12-SD	0.80
GFRP specimens	
G-D-12-NG	0.70
G-D-12-SD	0.75
G-SC-12-NG	0.91
G-SC-12-SD	0.93
CFRP specimens	
C-D-12-NG	0.53
C-D-12-SD	0.49

Finally, this study demonstrates the promising use of the BFRP bars in NSM applications. The tests confirm the superiority of the epoxy adhesives over the cementitious grouts in developing the bond strength of the NSM-FRP systems. The obtained results numerate the main parameters that affect the bond behavior of the NSM bars. Future work should build on those results to investigate the performance of large-scale reinforced concrete members strengthened with NSM systems. Lastly, those results should not be extended to other types of NSM-FRP bars prior to a thorough experimental investigation.

CRediT authorship contribution statement

Omar Aljidda: Methodology, Investigation, Data curation, Formal analysis, Writing – original draft. **Ahmed El Refai:** Visualization, Conceptualization, Methodology, Project administration, Supervision, Validation, Writing – review & editing. **Wael Alnahhal:** Supervision, Conceptualization, Visualization, Methodology, Project administration, Validation, Writing – review & editing.

Declaration of Competing Interest

The authors declare that they have no known competing financial interests or personal relationships that could have appeared to influence the work reported in this paper.

Data availability

Data will be made available on request.

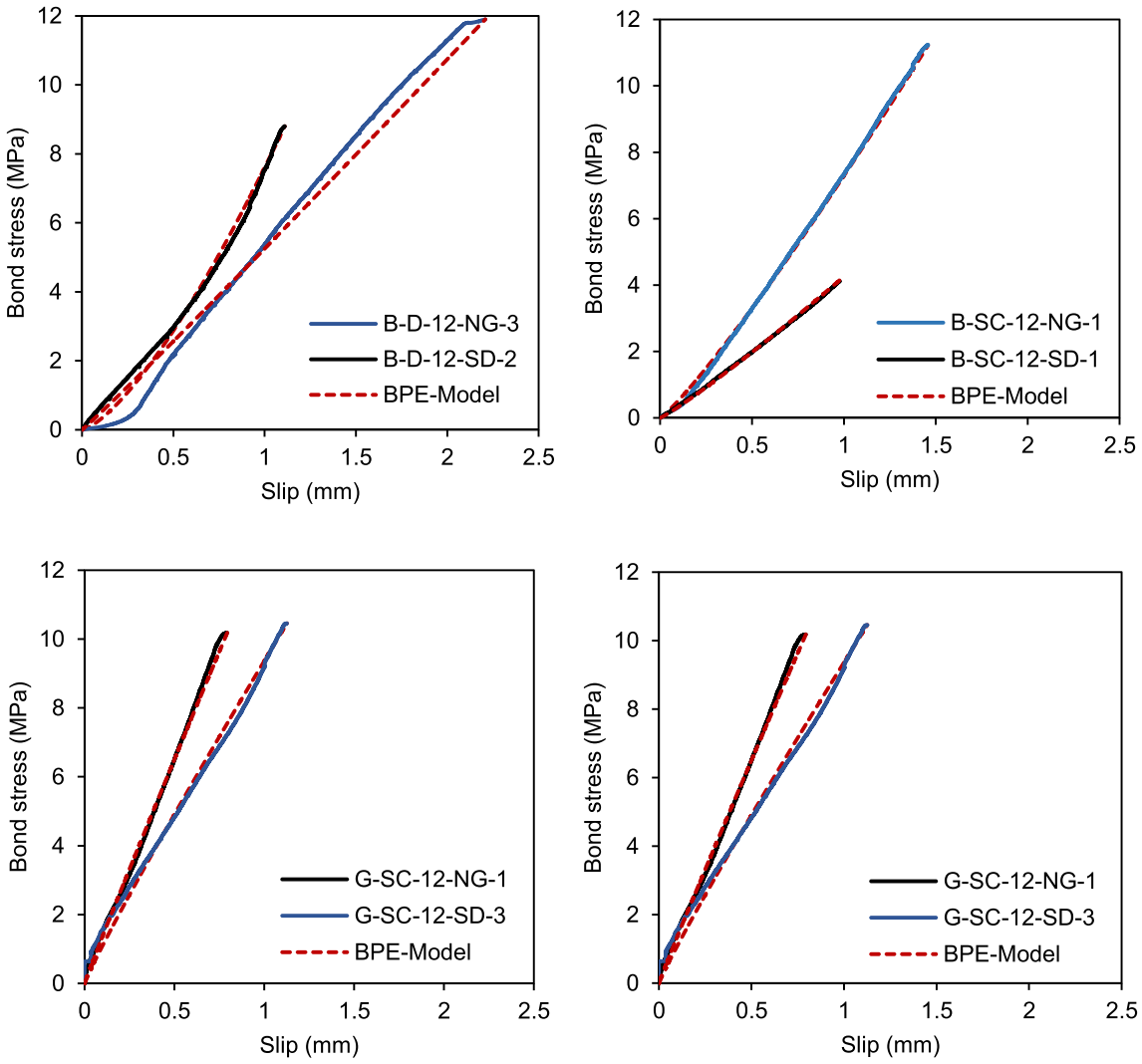

Fig. 17. Experimental versus analytical bond stress-slip relationships.

Acknowledgment

The authors would like to acknowledge the financial support provided by Qatar University (Fund No. QUST-1-CENG-2020-17) rewarded by the third author and the Natural Sciences and Engineering Research Council of Canada (NSERC) through their Discovery Grants Program - Award No. RGPIN-2017-04278 rewarded by the second author.

Data availability

Data availability the raw/processed data required to reproduce these findings cannot be shared at this time as the data also forms part of an ongoing study.

References:

[1] H. Maljaee, B. Ghiassi, P.B. Lourenço, Bond behavior in NSM-strengthened masonry, Eng Struct 166 (2018) 302–313, https://doi.org/10.1016/j.engstruct.2018.03.091.
[2] J. Gómez, L. Torres, C. Barris, Characterization and simulation of the bond response of NSM FRP reinforcement in Concrete, Materials 13 (2020), https://doi.org/10.3390/MA13071770.
[3] D.G. Novidis, S.J. Pantazopoulou, Bond tests of short NSM-FRP and steel bar anchorages, J. Compos. Constr. 12 (2008) 323–333, https://doi.org/10.1061/(ASCE)1090-0268(2008)12:3(323).
[4] W.K.K.G. Kalupahana, T.J. Ibell, A.P. Darby, Bond characteristics of near surface mounted CFRP bars, Constr Build Mater 43 (2013) 58–68, https://doi.org/10.1016/j.conbuildmat.2013.01.021.
[5] A. Bilotta, F. Ceroni, M. di Ludovico, E. Nigro, M. Pecce, G. Manfredi, Bond Efficiency of EBR and NSM FRP Systems for Strengthening Concrete Members, J. Compos. Constr. 15 (2011) 757–772, https://doi.org/10.1061/(asce)cc.1943-5614.0000204.
[6] L. De Lorenzis, J.G. Teng, Near-surface mounted FRP reinforcement: An emerging technique for strengthening structures, Compos B Eng 38 (2007) 119–143, https://doi.org/10.1016/j.compositesb.2006.08.003.
[7] L. De Lorenzis, A. Nanni, Characterization of FRP Rods as Near-Surface Mounted Reinforcement, J. Compos. Constr. 5 (2001) 114–121, https://doi.org/10.1061/(asce)1090-0268(2001)5:2(114).
[8] X. Wang, L. Cheng, Bond characteristics and modeling of near-surface mounted CFRP in concrete, Compos Struct 255 (2021), 113011, https://doi.org/10.1016/j.compstruct.2020.113011.
[9] J. Gómez, C. Barris, Y. Jahani, M. Baena, L. Torres, Experimental study and numerical prediction of the bond response of NSM CFRP laminates in RC elements under sustained loading, Constr Build Mater 288 (2021), https://doi.org/10.1016/j.conbuildmat.2021.123082.
[10] S.M. Al-Obaidi, Y.M. Saeed, F.N. Rad, Pullout Tests on Near-Surface-Mounted CFRP Rods with and Without Lateral Grooves, International Journal of Engineering & Technology 7 (2018) 72. https://doi.org/10.14419/ijet.v7i4.20.25855.
[11] M. Emara, C. Barris, M. Baena, L. Torres, J. Barros, Bond behavior of NSM CFRP laminates in concrete under sustained loading, Constr Build Mater 177 (2018) 237–246, https://doi.org/10.1016/j.conbuildmat.2018.05.050.
[12] R. Capozucca, M.G. Blasi, V. Corina, NSM technique: Bond of CFRP rods and static/dynamic response of strengthened RC beams, Compos Struct 127 (2015) 466–479, https://doi.org/10.1016/j.compstruct.2015.03.013.
[13] H. Peng, H. Hao, J. Zhang, Y. Liu, C.S. Cai, Experimental investigation of the bond behavior of the interface between near-surface-mounted CFRP strips and concrete, Constr Build Mater 96 (2015) 11–19, https://doi.org/10.1016/j.conbuildmat.2015.07.156.

[14] D. Lee, L. Cheng, J. Yan-Gee Hui, Bond Characteristics of Various NSM FRP Reinforcements in Concrete, J. Compos. Constr. 17 (2013) 117–129, https://doi.org/10.1061/(asce)cc.1943-5614.0000318.
[15] L. Torres, I.A. Sharaky, C. Barris, M. Baena, Experimental study of the influence of adhesive properties and bond length on the bond behaviour of NSM FRP bars in concrete, J. Civ. Eng. Manag. 22 (2016) 808–817, https://doi.org/10.3846/13923730.2014.914097.
[16] I.A. Sharaky, L. Torres, M. Baena, C. Miàs, An experimental study of different factors affecting the bond of NSM FRP bars in concrete, Compos Struct 99 (2013) 350–365, https://doi.org/10.1016/j.compstruct.2012.12.014.
[17] J.M.S. Cruz J. a O. Barros, Bond Behavior of Carbon Laminate Strips Into Concrete By Pullout-Bending Tests in: "Bond in Concrete – from Research to Standards" 2002 Budapest 8.
[18] X. Wang, L. Cheng, Bond characteristics and modeling of near-surface mounted CFRP in concrete, Compos Struct 255 (2021), https://doi.org/10.1016/j.compstruct.2020.113011.
[19] S.M. Soliman E. El-Salakawy B. Benmokrane Bond performance of near surface mounted FRP bars Journal of Composites for Construction. 15 2011 103 111 https://doi.org/1090-0268/2001/1-103-111/$25.00.
[20] J. Ricardo Cruz, J. Sena-Cruz, M. Rezazadeh, S. Seręga, E. Pereira, A. Kwiecień, B. Zając, Bond behaviour of NSM CFRP laminate strip systems in concrete using stiff and flexible adhesives, Compos Struct 245 (2020), https://doi.org/10.1016/j.compstruct.2020.112369.
[21] Z. Zhu, E. Zhu, Z. Chen, The Experiment Analysis of Bonding Performance between Near Surface Mounted CFRP Strip and Concrete at Different Curing Temperatures, Urban Rail, Transit 4 (2018) 155–162, https://doi.org/10.1007/s40864-018-0085-5.
[22] A. Al-Abdwais, R. Al-Mahaidi, Bond behaviour between NSM CFRP laminate and concrete using modified cement-based adhesive, Constr Build Mater 127 (2016) 284–292, https://doi.org/10.1016/j.conbuildmat.2016.09.142.
[23] F. Al-Mahmoud, A. Castel, R. François, C. Tourneur, Anchorage and tension-stiffening effect between near-surface-mounted CFRP rods and concrete, Cem Concr Compos 33 (2011) 346–352, https://doi.org/10.1016/j.cemconcomp.2010.10.016.
[24] J.M.S. Cruz, J.A.O., Barros,, Bond between near-surface mounted carbon-fiber-reinforced polymer laminate strips and concrete, J. Compos. Constr. 8 (2004) 519–527, https://doi.org/10.1061/(ASCE)1090-0268(2004)8.
[25] Q. Wang, H. Zhu, T. Li, G. Wu, X. Hu, Bond performance of NSM FRP bars in concrete with an innovative additional ribs anchorage system: An experimental study, Constr Build Mater 207 (2019) 572–584, https://doi.org/10.1016/j.conbuildmat.2019.02.020.
[26] W. Chen, F. Meng, H. Sun, Z. Guo, Bond behaviors of BFRP bar-to-concrete interface under dynamic loading, Constr Build Mater 305 (2021), 124812, https://doi.org/10.1016/j.conbuildmat.2021.124812.
[27] A. El Refai, M.-A. Ammar, R. Masmoudi, Bond Performance of Basalt Fiber-Reinforced Polymer Bars to Concrete, J. Compos. Constr. 19 (2014) 04014050, https://doi.org/10.1061/(asce)cc.1943-5614.0000487.
[28] R. Zou, F. Liu, Z. Xiong, S. He, L. Li, W. Wei, Experimental study on fatigue bond behaviour between basalt fibre-reinforced polymer bars and recycled aggregate concrete, Constr Build Mater 270 (2021), https://doi.org/10.1016/j.conbuildmat.2020.121399.
[29] Z. Xiong, W. Wei, F. Liu, C. Cui, L. Li, R. Zou, Y. Zeng, Bond behaviour of recycled aggregate concrete with basalt fibre-reinforced polymer bars, Compos Struct 256 (2021), https://doi.org/10.1016/j.compstruct.2020.113078.
[30] Z. Lu, L. Su, J. Lai, J. Xie, B. Yuan, Bond durability of BFRP bars embedded in concrete with fly ash in aggressive environments, Compos Struct 271 (2021), 114121, https://doi.org/10.1016/j.compstruct.2021.114121.
[31] A. Taha, W. Alnahhal, N. Alnuaimi, Bond durability of basalt FRP bars to fiber reinforced concrete in a saline environment, Compos Struct 243 (2020), https://doi.org/10.1016/j.compstruct.2020.112277.
[32] A. Altalmas, A. el Refai, F. Abed, Bond degradation of basalt fiber-reinforced polymer (BFRP) bars exposed to accelerated aging conditions, Constr Build Mater 81 (2015) 162–171, https://doi.org/10.1016/j.conbuildmat.2015.02.036.
[33] Z. Xiong, G. Mai, S. Qiao, S. He, B. Zhang, H. Wang, K. Zhou, L. Li, Fatigue bond behaviour between basalt fibre-reinforced polymer bars and seawater sea-sand concrete, Ocean Coast Manag 218 (2022), https://doi.org/10.1016/j.ocecoaman.2022.106038.
[34] S. Liu, X. Wang, Y.M.S. Ali, C. Su, Z. Wu, Flexural behavior and design of under-reinforced concrete beams with BFRP and steel bars, Eng Struct 263 (2022), 114386, https://doi.org/10.1016/j.engstruct.2022.114386.
[35] X. Wang, S. Liu, Y. Shi, Z. Wu, W. He, Integrated High-Performance Concrete Beams Reinforced with Hybrid BFRP and Steel Bars, J. Struct. Eng. 148 (2022), https://doi.org/10.1061/(asce)st.1943-541x.0003207.
[36] Z. Dong, G. Wu, H. Zhu, Y. Wei, X.L. Zhao, X. Shao, Bond and flexural performance of basalt fiber–reinforced polymer bar–reinforced seawater sea sand glass aggregate concrete beams, Adv. Struct. Eng. 24 (2021) 3359–3374, https://doi.org/10.1177/13694332211026228.
[37] F. Abed, M. Al-Mimar, S. Ahmed, Performance of BFRP RC beams using high strength concrete, Composites Part C: Open Access 4 (2021), 100107, https://doi.org/10.1016/j.jcomc.2021.100107.
[38] A. Abushanab, W. Alnahhal, M. Farraj, Structural performance and moment redistribution of basalt FRC continuous beams reinforced with basalt FRP bars, Eng Struct 240 (2021), 112390, https://doi.org/10.1016/j.engstruct.2021.112390.
[39] K. Attia, A. el Refai, W. Alnahhal, Flexural Behavior of Basalt Fiber-Reinforced Concrete Slab Strips with BFRP Bars: Experimental Testing and Numerical Simulation, J. Compos. Constr. 24 (2020) 04020007, https://doi.org/10.1061/(asce)cc.1943-5614.0001002.
[40] A. El Refai, W. Alnahhal, A. Al-Hamrani, S. Hamed, Shear performance of basalt fiber-reinforced concrete beams reinforced with BFRP bars, Compos Struct 288 (2022), 115443, https://doi.org/10.1016/j.compstruct.2022.115443.
[41] A. Al-Hamrani, W. Alnahhal, A. Elahtem, Shear behavior of green concrete beams reinforced with basalt FRP bars and stirrups, Compos Struct 277 (2021), 114619, https://doi.org/10.1016/j.compstruct.2021.114619.
[42] F. Abed, A. el Refai, S. Abdalla, Experimental and finite element investigation of the shear performance of BFRP-RC short beams, Structures 20 (2019) 689–701, https://doi.org/10.1016/j.istruc.2019.06.019.
[43] D. Tomlinson, A. Fam, Performance of Concrete Beams Reinforced with Basalt FRP for Flexure and Shear, J. Compos. Constr. 19 (2015) 04014036, https://doi.org/10.1061/(asce)cc.1943-5614.0000491.
[44] N. Elmesalami, F. Abed, A. el Refai, Concrete Columns Reinforced with GFRP and BFRP Bars under Concentric and Eccentric Loads: Experimental Testing and Analytical Investigation, J. Compos. Constr. 25 (2021) 04021003, https://doi.org/10.1061/(asce)cc.1943-5614.0001115.
[45] N. Elmessalami, A. el Refai, F. Abed, Fiber-reinforced polymers bars for compression reinforcement: A promising alternative to steel bars, Constr Build Mater 209 (2019) 725–737, https://doi.org/10.1016/j.conbuildmat.2019.03.105.
[46] ACI 440.2R, Guide for the design and construction of externally bonded FRP systems for strengthening concrete structures, American Concrete Institute, Farmington Hills, MI, USA, 2017.
[47] Astm d7205, d7205m-21, Standard Test Method for Tensile Properties of Fiber Reinforced Polymer Matrix Composite Bars 1, 100 Barr Harbor Drive, PO Box C700, West Condhohocken 2021 United States 10.1520/D7205_D7205M-21 PA 19428–2959.
[48] Astm c39, c39m, Standard Test Method for Compressive Strength of Cylindrical Concrete Specimens, 100 Barr Harbor drive, PO Box C700, West Conshohocken 2021 United States 10.1520/C0039_C0039M-21 PA 19428–2959.
[49] Astm c78, c78m, Standard Test Method for Flexural Strength of Concrete (Using Simple Beam with Third-Point Loading) 1, 100 Barr Harbor Drive, PO Box C700, West Conshohocken 2021 United states 10.1520/C0078_C0078M-21 PA 19428–2959.
[50] ISO, INTERNATIONAL STANDARD iTeh STANDARD iTeh STANDARD PREVIEW, International Organization for Standardization. 10406–1:20 (2015) 3–6.
[51] S. Solyom, G.L. Balázs, Bond of FRP bars with different surface characteristics, Constr Build Mater 264 (2020), https://doi.org/10.1016/j.conbuildmat.2020.119839.
[52] M.R.F. Coelho, J.M. Sena-Cruz, L.A.C. Neves, A review on the bond behavior of FRP NSM systems in concrete, Constr Build Mater 93 (2015) 1157–1169, https://doi.org/10.1016/j.conbuildmat.2015.05.010.
[53] D. Galati, L. de Lorenzis, Effect of construction details on the bond performance of NSM FRP bars in concrete, Adv. Struct. Eng. 12 (2009) 683–700, https://doi.org/10.1260/136943309789867836.
[54] W.K.K.G. Kalupahana, Anchorage and Bond Behaviour of Near Surface Mounted Fibre Reinforced Polymer Bars, 2009.
[55] L. De Lorenzis, A. Nanni, Bond between near-surface mounted fiber-reinforced polymer rods and concrete in structural strengthening, ACI Struct J 99 (2002) 123–132. https://doi.org/10.14359/11534.
[56] R. Eligehausen, E.P. Popov, V.V. Bertero, Local bond stress-slip relationships of deformed bars under generalized excitations, University of California, report no UCB/EERC-83/23 of the National Science Foundation, 1983.
[57] M. Aiello, Bond Performances of FRP Rebars-Reinforced concrete, J. Mater. Civ. Eng. 19 (2007) 205–213, https://doi.org/10.1061/(ASCE)0899-1561(2007)19.
[58] A. Taha, W. Alnahhal, N. Alnuaimi, Bond durability of basalt FRP bars to fiber reinforced concrete in a saline environment, Compos Struct 243 (2020), 112277, https://doi.org/10.1016/j.compstruct.2020.112277.
[59] E. Cosenza, G. Manfredi, R. Realfonzo, Behavior and Modeling of Bond of FRP Rebars to Concrete, J. Compos. Constr. 1 (1997) 40–51, https://doi.org/10.1061/(asce)1090-0268(1997)1:2(40).
[60] L. De Lorenzis, A. Rizzo, A. la Tegola, A modified pull-out test for bond of near-surface mounted FRP rods in concrete, Compos B Eng 33 (2002) 589–603, https://doi.org/10.1016/S1359-8368(02)00052-5.